Analyst

Electronic Supplementary Information

Characterizing the Non-Paraxial Talbot Effect in Two-Dimensional Periodic Arrays of Plasmonic Gold Nanodisks by Differential Interference Contrast Microscopy

Geun Wan Kim,[a,b] Seong Ho Kang,[c] and Ji Won Ha[a,b]*

[a]Advanced Nano-Bio-Imaging and Spectroscopy Laboratory, Department of Chemistry, University of Ulsan, 93 Daehak-ro, Nam-gu, Ulsan 44610, Republic of Korea

[b]Energy Harvest-Storage Research Center (EHSRC), University of Ulsan, 93 Daehak-ro, Nam-gu, Ulsan 44610, Republic of Korea

[c]Department of Applied Chemistry and Institute of Natural Sciences, Kyung Hee University, Yongin-si, Gyeonggi-do 17104, Republic of Korea

*To whom correspondence should be addressed.

Ji Won Ha

Phone: +82-52-712-8012

Fax: +82-52-712-8002

E-mail: jwha77@ulsan.ac.kr

Supplementary Movies

Movie S1: A movie showing DIC imaging of the periodic 2D AuND arrays measured at 600 nm by scanning in the z-direction with a step size of 40 nm. The self-image patterns are periodically repeated along the longitudinal direction.

Movie S2: A movie showing DIC imaging of the periodic 2D AuND arrays measured at 540 nm by scanning in the z-direction with a step size of 40 nm. The self-image patterns are periodically repeated along the longitudinal direction.

Experimental Section

Fabrication and Characterizations

The periodic two-dimensional (2D) arrays of plasmonic AuNDs with large-scale periodicity were fabricated from Korea National NanoFab Center (Suwon, South Korea, https://www.kanc.re.kr). Structural characterization of the fabricated AuND arrays were carried out using a scanning electron microscope (SEM) (JSM6500F, JEOL, Japan). Furthermore, the transmission spectrum of the 2D patterns were recorded with a Varian Carry 300 UV-Vis spectrometer.

Differential Interference Contrast Microscopy

We performed DIC microscopy using a Nikon inverted microscope (ECLIPSE Ti-U, JAPAN). DIC microscopy consists of a set of two Nomarski prisms, two polarizers, and a quarter-waveplate. We illuminated the sample by an oil immersion condenser with a NA of 1.4. The DIC signals coming from the sample were collected by a Plan Apo oil-immersion objective (100×, NA=1.4). To obtain DIC images with high quality, we used an Andor EMCCD camera (iXon Ultra 897, UK).

DIC Imaging of the Periodic AuND Patterns in the z-direction

The sample was placed onto the microscope stge. The DIC images of the patterns at the two illumination wavelengths (540 nm, 600 nm) were obtained by using a motorized rotary stage from Sigma Koki (SGSP-60YAM) coupled to the fine-adjustment knob on the microscope. The motor was controlled by Intelligent Driver, CSG-602R (Sigma Koki). We scanned in the z-

direction with a vertical step size of ~40 nm. The DIC images were recorded with the Andor EMCCD camera (iXon Ultra 897, UK), and the collected images were analyzed with MATLAB and NIH ImageJ.

Supplementary Figures

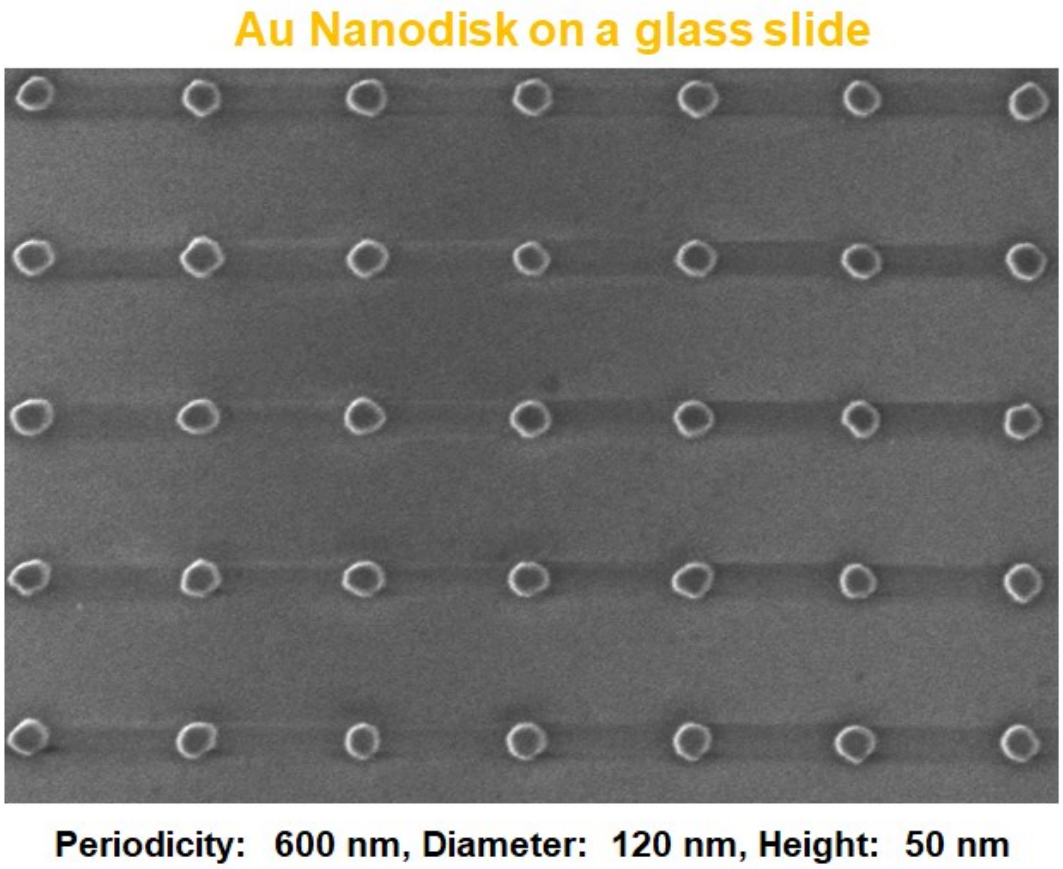

Fig. S1 SEM image of the periodic 2D arrays of AuNDs in large area.

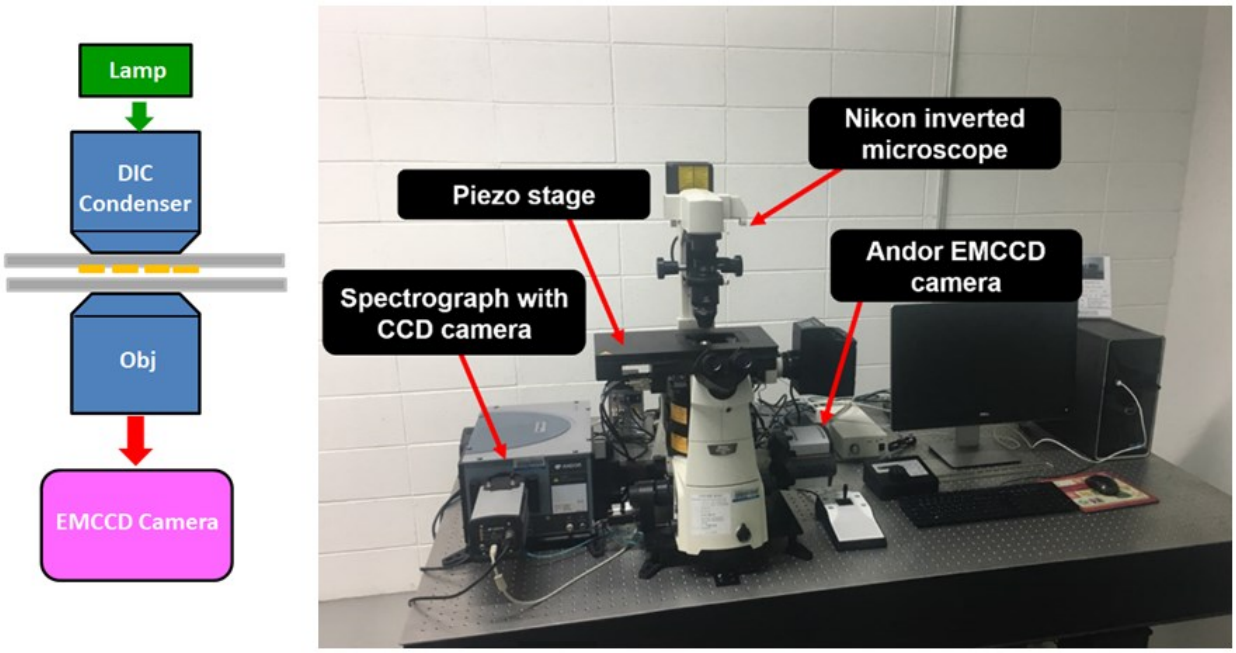

Fig. S2 Photograph to show the experimental setup for single particle spectroscpy and differential interference contrast microscopy.

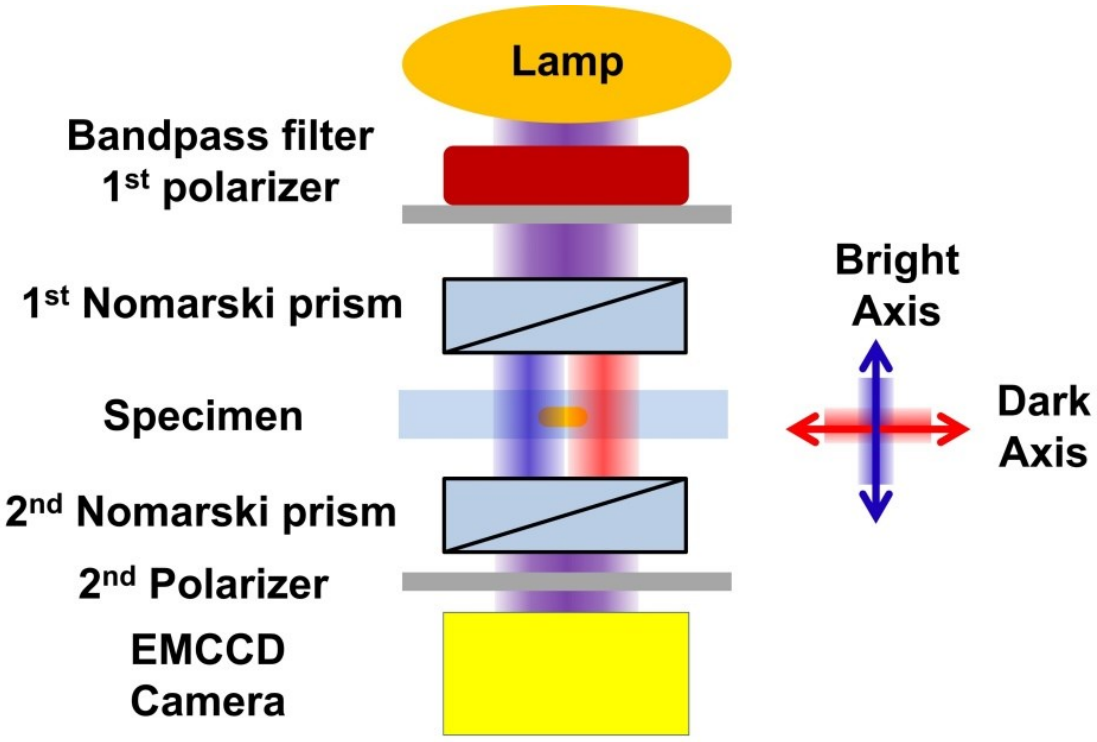

Fig. S3 The working principle of DIC microscopy. The incident light is split into two orthogonally linearly polarized beams by the first Nomarski prism. Two beams pass through the sample and are recombined by the second Nomarski prism to creat an interference pattern.

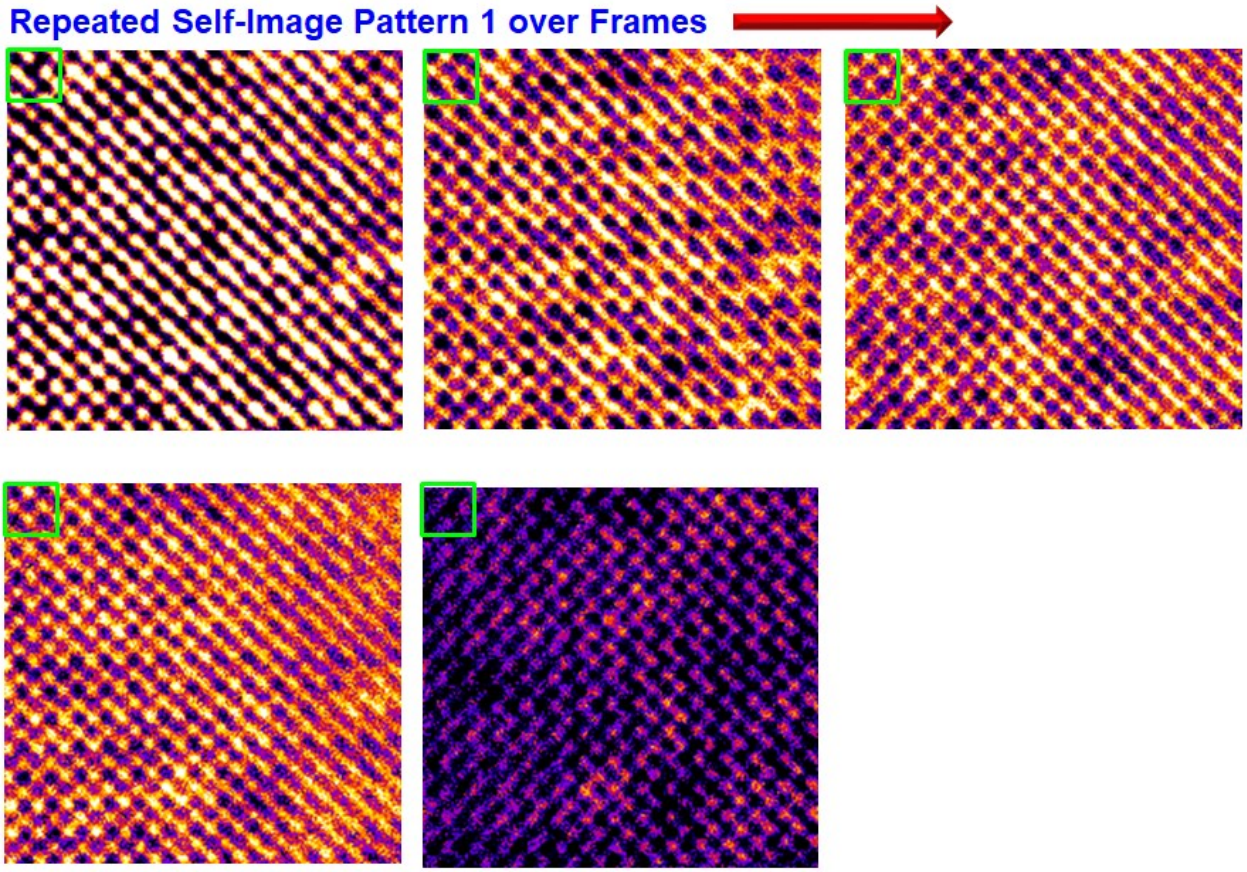

Fig. S4 Revivals of the self-image pattern 1 at 600 nm in the *z*-direction over frames under DIC microscopy.

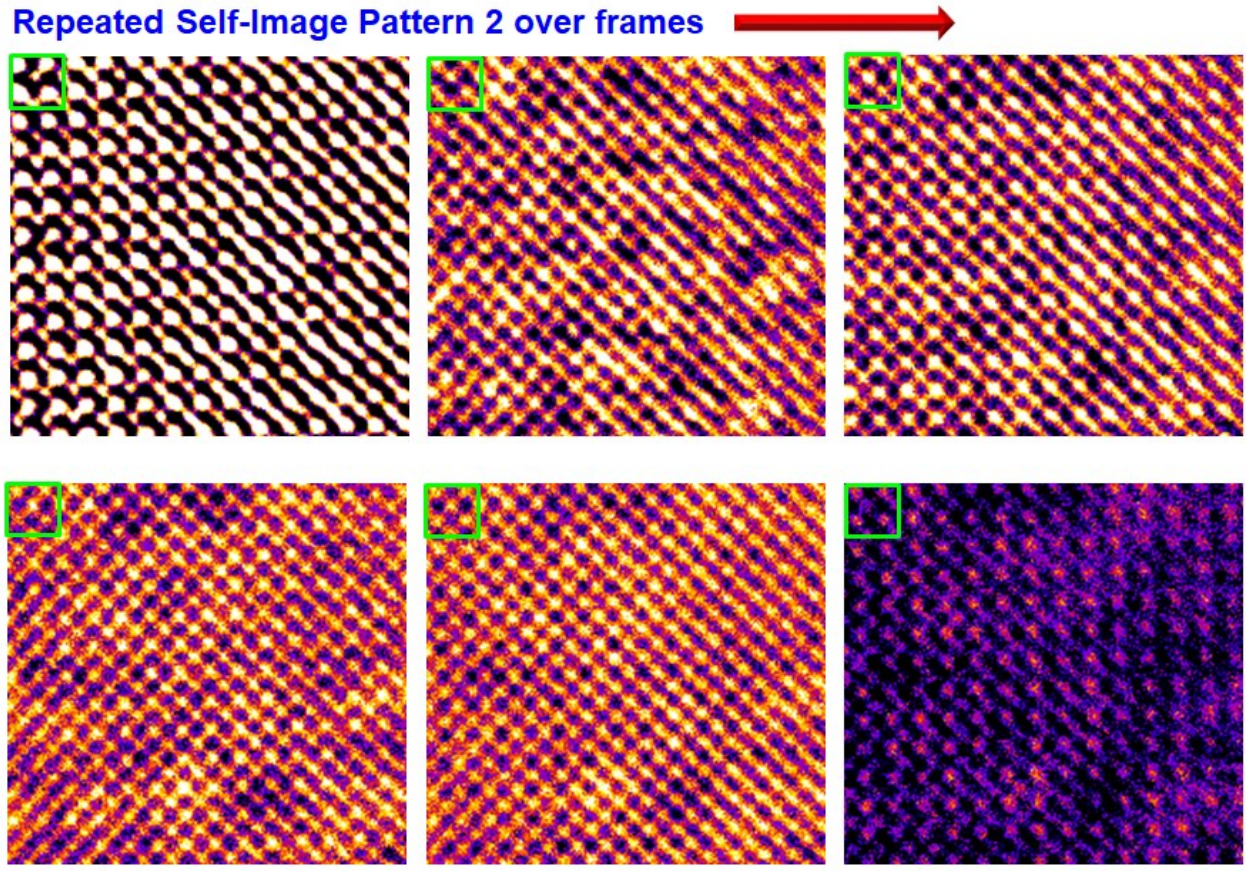

Fig. S5 Revivals of the self-image pattern 2 at 600 nm in the z-direction over frames under DIC microscopy.

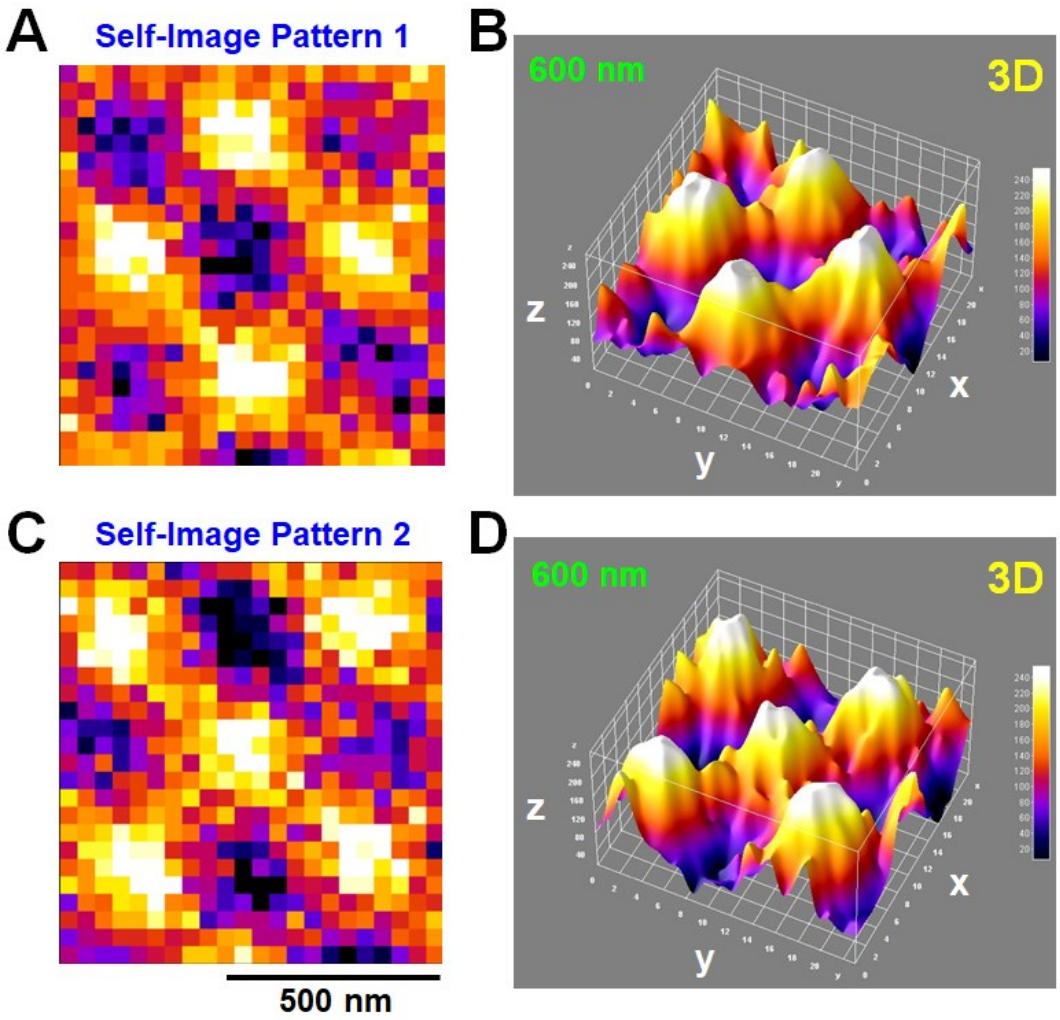

Fig. S6 (A, B) 2D and 3D images of the self-image pattern 1 in the periodic AuND arrays at 600 nm. **(C, D)** 2D and 3D images of the self-image pattern 2 in the periodic AuND arrays at 600 nm.

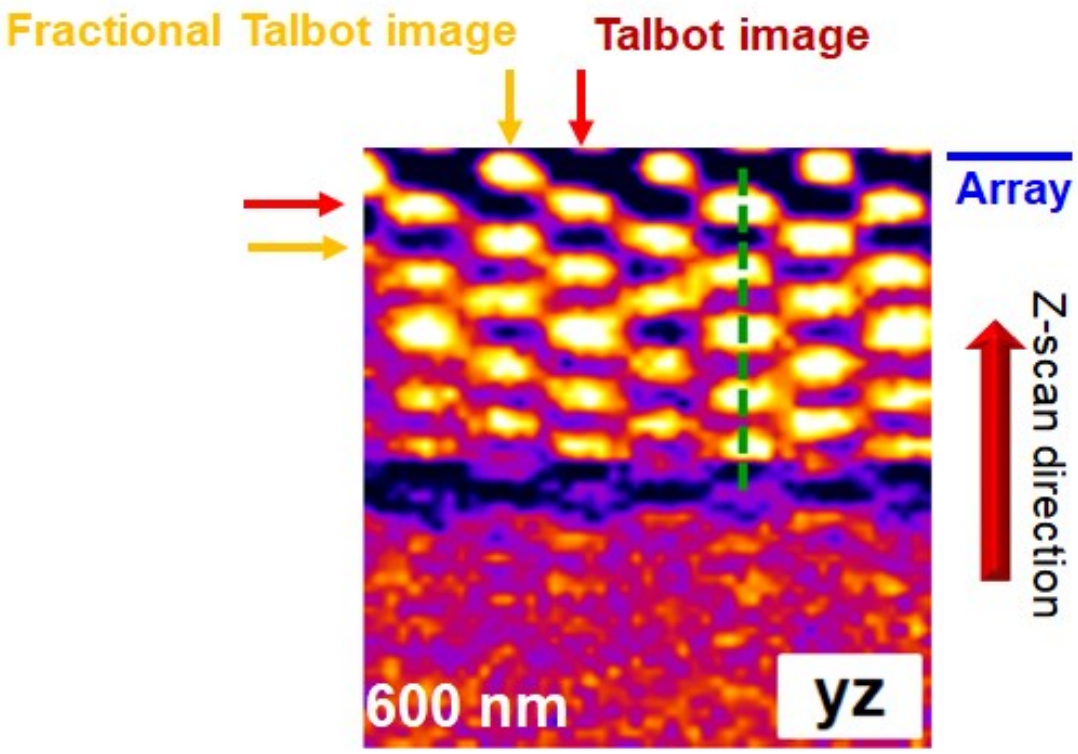

Fig. S7 The revivals of two kinds of self-image patterns (Talbot and fractional Talbot patterns) in the *y*-*z* plane at 600 m beyond the paraxial limit. The fractional Talbot patterns are observed at about half the Talbot distance (q=1, s=2) along the longitudinal direction.

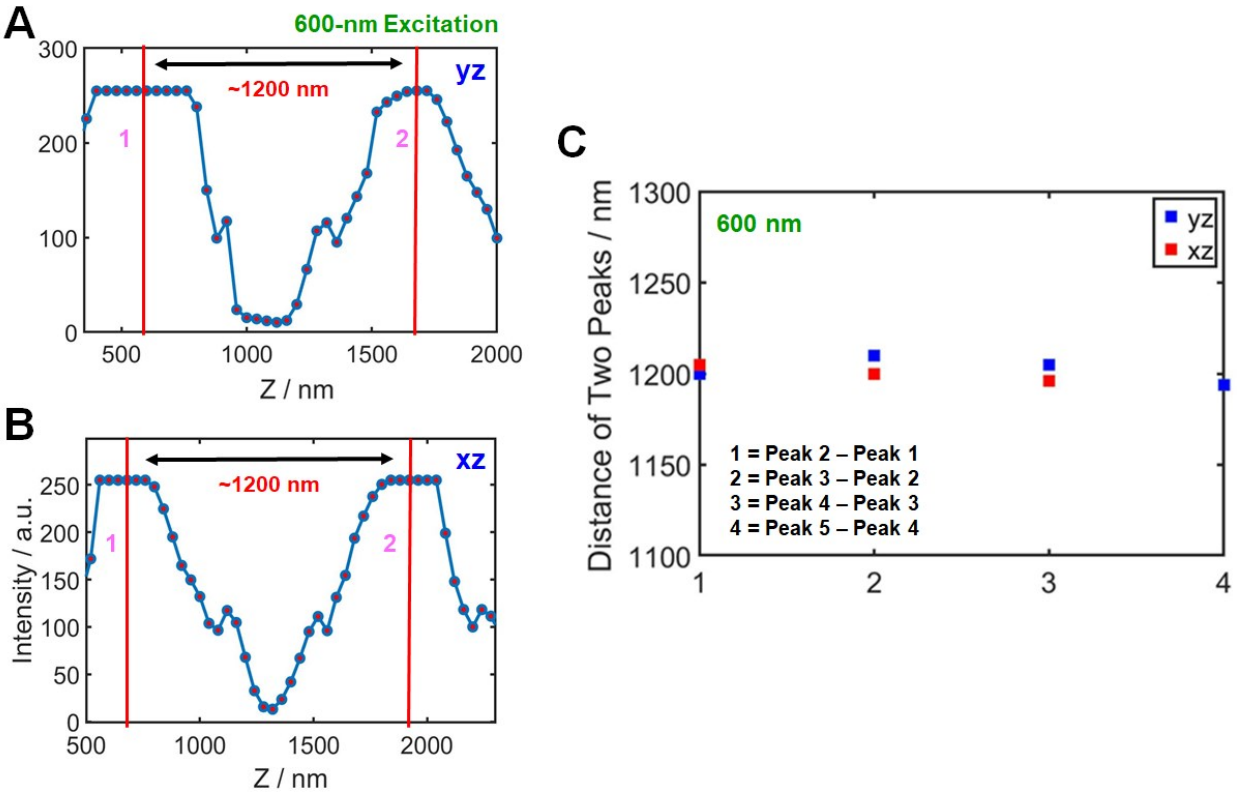

Fig. S8 (A, B) Cross-sectional intensity profile along the green-dotted lines in the *y*-*z* plane (A) and the *x*-*z* plane (B) of Figure 3B. The non-paraxial Talbot distance in the water medium measured at 600 nm (λ_{eff} = 451 nm, a_o/λ_{eff} =1.33) was determined to be about 1.22 μm. **(C)** The measured non-paraxial distances among the pink peaks in the *y*-*z* and *x*-*z* planes in Figures 3C and 3D.

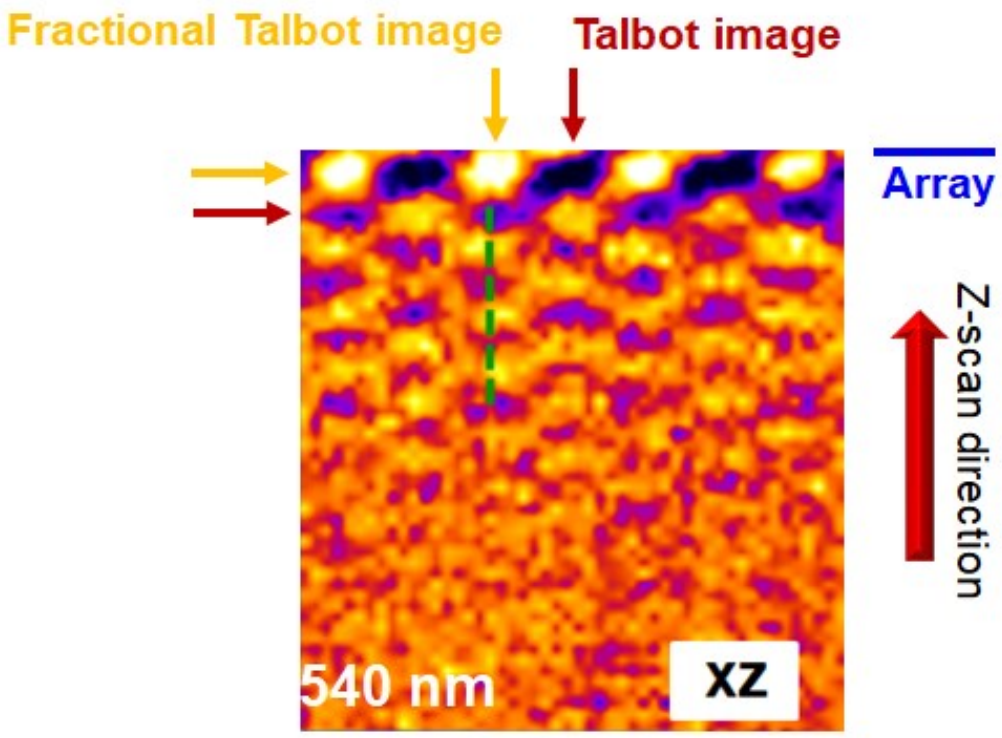

Fig. S9 The revivals of two kinds of self-image patterns (Talbot and fractional Talbot patterns) in the *x*-*z* plane at 540 m beyond the paraxial limit. The fractional Talbot patterns are observed at about half the Talbot distance (q=1, s=2) along the longitudinal direction.

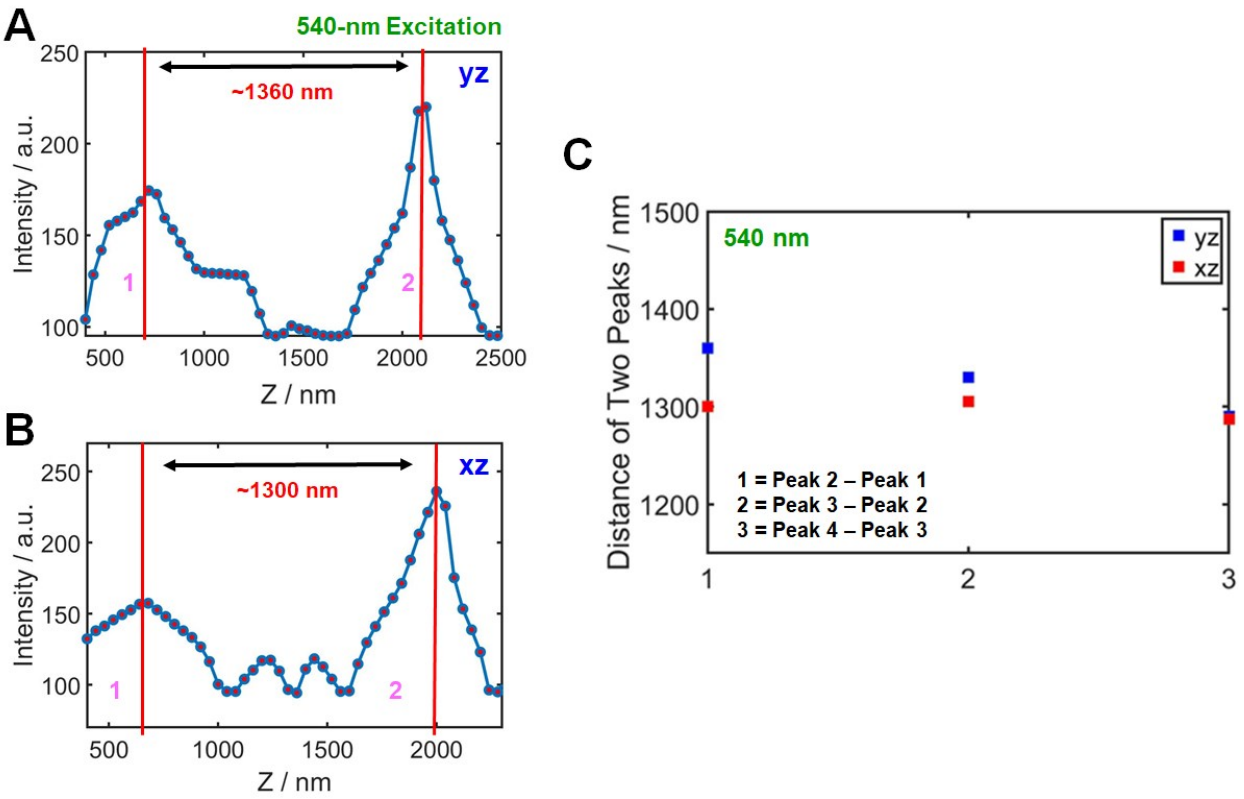

Fig. S10 (A, B) Cross-sectional intensity profile along the green-dotted lines in the *y*-*z* plane (A) and the *x*-*z* plane (B) of Figure 4B. The non-paraxial Talbot distance in the water medium measured at 540 nm (λ_{eff} = 406 nm, a_o/λ_{eff} =1.48) was determined to be about 1.34 μm. **(C)** The measured non-paraxial distances among the pink peaks in the *y*-*z* and *x*-*z* planes in Figures 4C and 4D.